ResearchGate

See discussions, stats, and author profiles for this publication at: https://www.researchgate.net/publication/231231442

1-D, 2-D, and 3-D Organic–Inorganic Hybrids Assembled from Keggin-type Polyoxometalates and 3d–4f Heterometals

ARTICLE *in* CRYSTAL GROWTH & DESIGN · JULY 2011

Impact Factor: 4.89 · DOI: 10.1021/cg2001249

CITATIONS
72

READS
9

6 AUTHORS, INCLUDING:

Shaowei Zhang
Hunan University of Science and Technology
17 PUBLICATIONS **210** CITATIONS

SEE PROFILE

Available from: Shaowei Zhang
Retrieved on: 02 February 2016

CRYSTAL GROWTH & DESIGN

ARTICLE

pubs.acs.org/crystal

1-D, 2-D, and 3-D Organic−Inorganic Hybrids Assembled from Keggin-type Polyoxometalates and 3d-4f Heterometals

Jingyang Niu, Shaowei Zhang, Huanni Chen, Junwei Zhao, Pengtao Ma, and Jingping Wang*

Institute of Molecular and Crystal Engineering, College of Chemistry and Chemical Engineering, Henan University Kaifeng, Henan 475004 P. R. China

Supporting Information

ABSTRACT: A series of organic−inorganic hybrid polyoxometalate derivatives $\{[Cu(en)_2]_{1.5}[Cu(en)(2,2'\text{-bipy})(H_2O)_n]Ce[(\alpha\text{-}PW_{11}O_{39})_2]\}^{6-}$ [(Ln, n) = (Ce^{III}, 0) for **1**, (Pr^{III}, 1) for **2**)], $\{[Cu(en)_2]_2(H_2O)[Cu(en)(2,2'\text{-bipy})]Ln[(\alpha\text{-}HPW_{11}O_{39})_2]\}^{4-}$ [Ln = Gd^{III} for **3**, Tb^{III} for **4**, Er^{III} for **5**] and $\{[Cu(en)_2]_{1.5}[Cu(en)(2,2'\text{-bipy})]Nd[(\alpha\text{-}H_5PW_{11}O_{39})_2]\}^{3-}$ for **6** (2,2′-bipy =2, 2′-bipyridine and en = ethylenediamine) have been successfully synthesized under hydrothermal conditions and further characterized by elemental analyses, inductively coupled plasma (ICP) analyses, X-ray powder diffraction (XRPD), IR spectra, UV spectra, electron paramagnetic resonance (EPR) spectra, thermogravimetric (TG) analyses, and single-crystal X-ray diffraction. The common features of **1**−**6** are that they all consist of sandwich-type $[Ln(\alpha\text{-}PW_{11}O_{39})_2]^{11-}$ polyoxoanions as the fundamental building blocks and copper coordination cations as bridges. **1** and **2** show the 1-D zigzag chains, and **3**−**5** exhibit the unprecedented 2-D structures built by $[Ln(\alpha\text{-}PW_{11}O_{39})_2]^{11-}$ polyoxoanions and $[Cu(en)_2]^{2+}$ and $[Cu(en)(2,2'\text{-bpy})]^{2+}$ cations, whereas **6** displays the scarce 3-D framework with a $(4^6\cdot6^4)$ topology. As expected, **1**−**6** contain two types of organic ligands. Furthermore, the photocatalysis properties of rhodamine-B (RhB) upon a 500 W Hg lamp irradiation in the presence of **1**, **2**, **3**, **4**, **5**, or **6** have been examined. The photoluminescence property of **4** has been investigated.

INTRODUCTION

The synthesis and exploitation of polyoxometalates (POMs) have attracted considerable attention in recent years, owing to not only their diversities of shape, size, and redox properties but also their potential applications in catalysis, photochemistry, electrochemistry, and magnetism.[1] Among POMs, lacunary Keggin species have attracted increasing attention, because they are often used as versatile building blocks to link transition-metal (TM) or lanthanide (Ln) cations to construct transition-metal substituted POMs (TMSPs) or lanthanide substituted POMs (LSPs). Hitherto, a large number of lacunary Keggin TMSPs have been reported.[2] Meanwhile, Keggin-type LSPs have been greatly investigated.[3] However, the investigation on the extended structures constructed by POMs and 3d-4f heterometals is very limited,[4] though lots of Ln−TM coordination polymers have been reported.[5] To our knowledge, the reports on Keggin-type POMs containing 3d-4f heterometals are very rare. In 2007, a Dy^{III}−V^{IV} heterometallic sandwich POM $[((VO)_2Dy(H_2O)_4K_2(H_2O)_2Na(H_2O)_2)(\alpha\text{-}B\text{-}AsW_9O_{33})_2]^{8-}$ was reported.[6] In the same year, Liu et al. isolated a family of 1-D 3d-4f organic−inorganic hybrids $[\{Ln(PW_{11}O_{39})_2\}\{Cu_2(bpy)_2(\mu\text{-}ox)\}]^{9-}$.[7] Subsequently, Wang's group synthesized a series of 3d-4f derivatives $[K\subset\{FeCe(AsW_{10}O_{38})(H_2O)_2\}_3]^{14-}$,[8a] $[\{Ce(H_2O)_7\}_2Mn_4Si_2W_{18}O_{68}(H_2O)_2]^{6-}$,[8b] $\{Nd_2(H_2O)_{12}Cu_4(H_2O)_2(SiW_9O_{34})_2\}^{6-}$.[8c] In 2009−2010, three unprecedented cubane-$\{LnCu_3(OH)_3O\}$ substituted monovacant $[\alpha\text{-}SiW_{11}O_{39}]^{8-}$ and a 1-D double-chain $[(\gamma\text{-}SiW_{10}O_{36})_2(Cr(OH)(H_2O))_3(La(H_2O)_7)_2]^{4-}$ were discovered by Mialane et al.[9] Very recently, a dimeric $[\{Ce(H_2O)_2\}_2Mn_2(B\text{-}\alpha\text{-}GeW_9O_{34})_2]^{8-}$ was isolated by Reinoso's group.[10]

Recently, we are focusing on the investigation on the reaction system containing POMs and 3d-4f heterometals, expecting to obtain novel 3d-4f heterometallic POMs. In this context, we choose lacunary Keggin-type POMs ($Na_9[\alpha\text{-}PW_9O_{34}]\cdot16H_2O$ and $Na_7[\alpha\text{-}PW_{11}O_{39}]\cdot nH_2O$), Ln^{III} ions, Cu^{II} ions, and mixed organic ligands (en and 2,2′-bipy) to construct organic−inorganic hybrid high-dimensional 3d-4f heterometallic Keggin-type POM-based derivatives based on the following considerations: (i) The lacunary sites on polyoxoanions (POAs) can work as structure-directing agents to induce novel structures. Thus, we have synthesized a series of Keggin-type LSPs built by lacunary Keggin-type POMs and Ln ions.[11] (ii) In contrast to other 3d TM ions, the Cu^{II} ion exhibits flexible coordination modes (square, trigonal bipyramid, square pyramid, and octahedron); moreover, the presence of the Jahn−Teller effect of the octahedron and the pseudo-Jahn−Teller effect of the square pyramid for the Cu^{II} ion can overcome steric hindrance to be favorable to form novel structures.[12] So, the Cu^{II} ion can be used. (iii) Most of the previously reported 3d-4f substituted POMs are inorganic and contain only one type of organic ligand; thus, they provide us a great opportunity for exploring 3d-4f substituted POMs containing mixed organic ligands. Recently, we simultaneously introduced aliphatic diamine ligands such as en and aromatic N-ligands such as 2,2′-bipy to our system to prepare novel 3d-4f heterometallic phosphotungstates with mixed organic ligands. Finally, six novel organic−inorganic hybrids, $\{[Cu(en)_2]_{1.5}[Cu(en)(2,2'\text{-bipy})(H_2O)_n]Ce[(\alpha\text{-}PW_{11}O_{39})_2]\}^{6-}$ [(Ln, n) = (Ce^{III}, 0) for **1**, (Pr^{III}, 1) for **2**)], $\{[Cu(en)_2]_2(H_2O)[Cu(en)(2,2'\text{-bipy})]Ln[(\alpha\text{-}HPW_{11}O_{39})_2]\}^{4-}$ [Ln = Gd^{III} for **3**, Tb^{III} for

Received: January 26, 2011
Revised: June 24, 2011
Published: July 15, 2011

ACS Publications © 2011 American Chemical Society

Table 1. Crystallographic Data and Structure Refinements for 1−6

	1	2	3	4	5	6
formula	$C_{26}H_{80}CeCu_{3.5}N_{18}O_{80}P_2W_{22}$	$C_{26}H_{93}Cu_{3.5}N_{18}O_{86.5}P_2PrW_{22}$	$C_{36}H_{101}Cu_5GdN_{20}O_{88}P_2W_{22}$	$C_{36}H_{102}Cu_5N_{20}O_{88.5}P_2TbW_{22}$	$C_{36}H_{102}Cu_5ErN_{20}O_{88.5}P_2W_{22}$	$C_{20}H_{59}Cu_3N_{12}Na_2NdO_{81}P_2W_{22}$
M_r (g mol^{-1})	6393.95	6511.83	6803.68	6814.36	6822.69	6251.23
T (K)	296(2)	296(2)	296(2)	296(2)	296(2)	296(2)
space group	$P\bar{1}$	$P\bar{1}$	$P\bar{1}$	$P\bar{1}$	$P\bar{1}$	$P\bar{1}$
crystal system	triclinic	triclinic	triclinic	triclinic	triclinic	triclinic
a (Å)	12.923(8)	13.0173(6)	13.7083(16)	13.7020(8)	13.7089(13)	15.563(12)
b (Å)	19.427(13)	19.3803(9)	19.323(2)	19.3240(10)	19.2704(18)	19.967(16)
c (Å)	21.115(14)	21.5028(9)	25.369(3)	25.3506(14)	25.333(2)	20.922(16)
α (deg)	95.816(11)	96.0070(10)	105.421(2)	105.3820(10)	105.130(2)	116.419(15)
β (deg)	93.135(11)	95.3110(10)	104.048(2)	104.0170(10)	104.1910(10)	91.769(15)
γ (deg)	96.147(11)	95.7130(10)	99.871(2)	99.9580(10)	99.847(2)	94.845(16)
V (Å^3)	5232(6)	5339.0(4)	6080.8(12)	6074.0(6)	6062.6(10)	5784(8)
Z	2	2	2	2	2	2
D_c (g cm^{-3})	4.056	4.048	3.715	3.714	3.737	3.586
μ (mm^{-1})	25.328	24.858	22.232	22.294	22.445	22.876
R_{int}	0.0787	0.0377	0.0946	0.0429	0.0298	0.0995
reflns collected	25472	27829	29833	31666	31396	29432
indep reflns	18017	18684	20156	21247	21249	20179
params	1339	1408	1576	1597	1588	1259
GOF on F^2	1.005	1.016	1.015	1.005	1.008	1.003
R_1, wR_2 [$I > 2\sigma(I)$]	0.0730, 0.1371	0.0440, 0.0866	0.0641, 0.1592	0.0443, 0.0831	0.0381, 0.0847	0.0842, 0.1528
R_1[a], wR_2 [all data]	0.1637, 0.1545	0.0669, 0.0932	0.0769, 0.1669	0.0692, 0.0913	0.0526, 0.0894	0.1479, 0.1570

4, Er^{III} for **5**], and $\{[Cu(en)_2]_{1.5}[Cu(en)(2,2'\text{-bipy})]Nd[(\alpha\text{-}H_5PW_{11}O_{39})_2]\}^{3-}$ for **6**, have been prepared. The common features of **1**−**6** are that they all consist of sandwich-type $[Ln(\alpha\text{-}PW_{11}O_{39})_2]^{11-}$ POAs as the fundamental building blocks and copper coordination cations as bridges. **1** and **2** show the 1-D zigzag chains, and **3**−**5** exhibit the unprecedented 2-D structures built by $[Ln(\alpha\text{-}PW_{11}O_{39})_2]^{11-}$ POAs and $[Cu(en)_2]^{2+}$ and $[Cu(en)(2,2'\text{-bipy})]^{2+}$ cations, whereas **6** displays the scarce 3-D framework with a $(4^6\cdot6^4)$ topology. As expected, **1**−**6** contain two types of organic ligands. Furthermore, the photocatalytic properties of the RhB upon a 500 W Hg lamp irradiation in the presence of **1**, **2**, **3**, **4**, **5**, or **6** have been examined. The photoluminescence property of **4** has been investigated.

EXPERIMENTAL SECTION

General Methods and Materials. $Na_9[\alpha\text{-}PW_9O_{34}]\cdot16H_2O$ and $Na_7[\alpha\text{-}PW_{11}O_{39}]\cdot nH_2O$ were prepared as described in the literature[13] and confirmed by IR spectra. Other chemical reagents were purchased without further purification. Elemental analyses (C, H, and N) were conducted on a Perkin-Elmer 2400-II CHNS/O analyzer. ICP analyses were performed on a Perkin-Elmer Optima 2000 ICP-OES spectrometer. IR spectra were obtained from a solid sample pelletized with KBr pellets on a Nicolet FT-IR 360 spectrometer in the range 4000−400 cm^{-1}. XRPD were performed on a Philips X'Pert-MPD instrument with Cu Kα radiation (λ = 1.54056 Å) in the range 2θ = 10−40° at 293 K. TG analyses were performed under a N_2 atmosphere on a Mettler-Toledo TGA/SDTA 851^e instrument with the heating rate 10 °C·min^{-1} from 25 to 800 °C. UV−vis spectra were obtained with a U-4100 spectrometer (distilled water as solvent) at 300 K. Photoluminescence measurements were performed on a SPEX SPEX·F212 fluorescence spectrophotometer. EPR spectra of **2**, **4**, and **5** were obtained on a Bruker ER-2000-DSRC10 spectrometer at the X-band at 300 and 110 K. Photocatalysis of **1**−**6** was carried out on a SGY-II multipurpose photoreactor (Stonetech Electric Equipment, Nanjing, China), and the light source was provided by a 500 W Hg lamp, which was positioned inside a cylindrical reactor, surrounding by a circulating water jacket to cool the lamp. The aqueous solution was prepared by adding 1.2 × 10^{-6} mol samples of **1**, **2**, **3**, **4**, **5**, or **6** to a 25 mL solution of RhB dye (2 × 10^{-5} mol·L^{-1}). Prior to irradiation, the suspensions were magnetically stirred in the dark for about 30 min to ensure a suitable equilibrium of the working systems. At given time intervals, 3 mL samples were taken out from the quartz glass tubes, centrifuged, and then filtered. The solution was analyzed by UV−visible spectroscopy.

Syntheses of $(enH_2)_2[Cu(en)_2]\{[Cu(en)_2]_{1.5}[Cu(en)(2,2'\text{-bipy})]Ce[(\alpha\text{-}PW_{11}O_{39})_2]\}\cdot2H_2O$ (**1**). $Na_9[\alpha\text{-}PW_9O_{34}]\cdot16H_2O$ (0.50 g, 0.18 mmol), $Na_7[\alpha\text{-}PW_{11}O_{39}]\cdot nH_2O$ (0.50 g, 0.17 mmol), $CeCl_3\cdot7H_2O$ (0.10 g, 0.27 mmol), $CuCl_2\cdot2H_2O$ (0.10 g, 0.59 mmol), and en (0.10 mL, 1.48 mmol) were successively dissolved in water (10 mL), and then a solution of ethanol (2 mL) containing 2,2′-bipy (0.04 g, 0.26 mmol) was added dropwise. After it was stirred for 3 h (the starting pH_i = 4.9), the resulting mixture was sealed in a 30 mL Telfon-lined stainless steel autoclave, kept at 170 °C for 4 days, and then slowly cooled to room temperature (the end pH_f = 5.6). Purple block crystals were collected by filtering, washed with distilled water, and dried in air. Yield: ca. 33% (based on $Na_7[\alpha\text{-}PW_{11}O_{39}]\cdot nH_2O$). Anal. Calcd (%) for **1**: C, 4.88; H, 1.28; N, 3.94; Cu, 3.48; Ce, 2.19; P, 0.97; W, 63.25. Found: C, 5.03; H, 1.39; N, 4.05; Cu, 3.64; Ce, 2.06; P, 0.83; W, 63.08. IR (KBr pellets): 3320 (w), 3258 (w), 1587 (m), 1460 (m), 1446 (s), 1385 (m), 1317 (w), 1253 (w), 1163 (w), 1094 (s), 1041 (s), 943 (s), 877 (s), 832 (s), 776 (s) cm^{-1}.

Synthesis of $(enH_2)_2[Cu(en)_2(H_2O)]\{[Cu(en)_2]_{1.5}[Cu(en)(2,2'\text{-bipy})(H_2O)]Pr[(\alpha\text{-}PW_{11}O_{39})_2]\}\cdot6.5H_2O$ (**2**). The preparation of **2** was similar to that of **1**, except that $PrCl_3\cdot7H_2O$ (0.10 g, 0.27 mmol) replaced $CeCl_3\cdot7H_2O$ (pH_i = 4.9, pH_f = 5.4). Yield: 35% (based on $Na_7[\alpha\text{-}PW_{11}O_{39}]\cdot nH_2O$). Anal. Calcd (%) for **2**: C, 4.80; H, 1.44; N, 3.87; Cu, 3.42; Pr, 2.16; P, 0.95; W, 62.11. Found: C, 4.89; H, 1.57; N, 3.98. Cu, 3.55; Pr, 2.02; P, 0.86; W, 62.37. IR (KBr pellets): 3306 (w),

dx.doi.org/10.1021/cg2001249 |Cryst. Growth Des. 2011, 11, 3769–3777

3247 (w), 1584 (m), 1460 (m), 1445 (s), 1385 (m), 1317 (w), 1250 (w), 1161 (w), 1094 (s), 1041 (s), 946 (s), 880 (s), 833 (s), 776 (s) cm^{-1}.

*Synthesis of $[Cu(en)_2(H_2O)_2][Cu(en)(2,2'\text{-bipy})(H_2O)]\{[Cu(en)_2]_2(H_2O)[Cu(en)(2,2'\text{-bipy})]Gd[(\alpha\text{-}HPW_{11}O_{39})_2]\}\cdot 6H_2O$ (**3**).* The preparation of **3** was similar to that of **1**, except that $GdCl_3\cdot 6H_2O$ (0.10 g, 0.27 mmol) replaced $CeCl_3\cdot 7H_2O$ (pH_i = 4.7, pH_f = 5.2). Yield: 38% (based on $Na_7[\alpha\text{-}PW_{11}O_{39}]\cdot nH_2O$). Anal. Calcd (%) for **3**: C, 6.36; H, 1.50; N, 4.12; Cu, 4.67; Gd, 2.31; P, 0.91; W, 59.45. Found: C, 6.48; H, 1.58; N, 4.21; Cu, 4.54; Gd, 2.17; P, 1.06; W, 59.72. IR (KBr pellets): 3309 (w), 3254 (w), 1587 (m), 1460 (m), 1446 (s), 1385 (m), 1320 (w), 1250 (w), 1163 (w), 1098 (s), 1043 (s), 948 (s), 879 (s), 835 (s), 778 (s) cm^{-1}.

*Synthesis of $[Cu(en)_2(H_2O)_2][Cu(en)(2,2'\text{-bipy})(H_2O)]\{[Cu(en)_2]_2[Cu(en)(2,2'\text{-bipy})]Tb[(\alpha\text{-}HPW_{11}O_{39})_2]\}\cdot 7.5H_2O$ (**4**).* The preparation of **4** was similar to that of **1**, except that $TbCl_3\cdot 6H_2O$ (0.10 g, 0.27 mmol) replaced $CeCl_3\cdot 7H_2O$ (pH_i = 4.6, pH_f = 4.9). Yield: 42% (based on $Na_7[\alpha\text{-}PW_{11}O_{39}]\cdot nH_2O$). Anal. Calcd (%) for **4**: C, 6.35; H, 1.51; N, 4.11; Cu, 4.66; Gd, 2.33; P, 0.91; W, 59.35. Found: C, 6.46; H, 1.60; N, 4.22; Cu, 4.55; Gd, 2.1; P, 1.03; W, 59.57. IR (KBr pellets): 3315 (w), 3255 (w), 1588 (m), 1460 (m), 1446 (s), 1382 (m), 1320 (w), 1248 (w), 1163 (w), 1100 (s), 1043 (s), 948 (s), 881 (s), 836 (s), 780 (s) cm^{-1}.

*Synthesis of $[Cu(en)_2(H_2O)][Cu(en)(2,2'\text{-bipy})(H_2O)]\{[Cu(en)_2]_2(H_2O)[Cu(en)(2,2'\text{-bipy})]Er[(\alpha\text{-}HPW_{11}O_{39})_2]\}\cdot 7.5H_2O$ (**5**).* The preparation of **5** was similar to that of **1**, except that $ErCl_3\cdot 6H_2O$ (0.10 g, 0.26 mmol) replaced $CeCl_3\cdot 7H_2O$ (pH_i = 4.9, pH_f = 6.5). Yield: 48% (based on $Na_7[\alpha\text{-}PW_{11}O_{39}]\cdot nH_2O$). Anal. Calcd (%) for **5**: C, 6.34; H, 1.51; N, 4.11; Cu, 4.66; Er, 2.45; P, 0.91; W, 59.28. Found: C, 6.46; H, 1.60; N, 4.23; Cu, 4.78; Er, 2.31; P, 0.78; W, 59.53. IR (KBr pellets): 3302 (w), 3252 (w), 1587 (m), 1460 (m), 1446 (s), 1383 (m), 1320 (w), 1250 (w), 1164 (w), 1103 (s), 1044 (s), 948 (s), 878 (s), 839 (s), 784 (s) cm^{-1}.

*Synthesis of $Na_2[Cu(en)_2]_{0.5}\{[Cu(en)_2]_{1.5}[Cu(en)(2,2'\text{-bipy})]Nd[(\alpha\text{-}H_5PW_{11}O_{39})_2]\}\cdot 3H_2O$ (**6**).* The preparation of **6** was similar to that of **1**, except that $NdCl_3\cdot 6H_2O$ (0.10 g, 0.28 mmol) replaced $CeCl_3\cdot 7H_2O$ (pH_i = 5.2, pH_f = 5.8). Yield: 37% (based on $Na_7[\alpha\text{-}PW_{11}O_{39}]\cdot nH_2O$). Anal. Calcd (%) for **6**: C, 3.84; H, 0.95; N, 2.69; Na, 0.74; Cu, 3.05; Nd, 2.31; P, 0.99; W, 64.70. Found: C, 3.99; H, 1.07; N, 2.83; Na, 0.58; Cu, 3.26; Nd, 2.45; P, 0.87; W, 65.53. IR (KBr pellets): 3308 (w), 3252 (w), 1589 (m), 1460 (m), 1446 (s), 1385 (m), 1320 (w), 1252 (w), 1163 (w), 1096 (s), 1040 (s), 946 (s), 883 (s), 833 (s), 777 (s) cm^{-1}.

X-ray Crystallography. Intensity data for **1**−**6** were collected on a Bruker Apex-II CCD diffractometer with Mo Kα monochromated radiation (λ = 0.71073 Å) at 296(2) K. Routine Lorentz polarization and empirical absorption corrections were applied. The structures were solved by direct methods and refined by full-matrix least-squares methods on F^2 with the SHELXTL-97 program package.[14] No hydrogen atoms associated with the water molecules were located from the difference Fourier map. Positions of the hydrogen atoms attached to the carbon and nitrogen atoms were geometrically placed. All hydrogen atoms were refined isotropically as a riding mode using the default SHELXTL parameters. A summary of crystallographic data and structural refinements for **1**−**6** is given in Table 1. CCDC reference nos. 808383−808388 for **1**−**6**, respectively. These data can be obtained free of charge from The Cambridge Crystallographic Data Centre via www.ccdc.cam.ac.uk/data_ request/cif.

RESULTS AND DISCUSSION

Synthesis. To our knowledge, 3d-4f heterometallic POMs remain less reported to date, but only one example of 3d-4f heterometallic POMs containing mixed ligands was isolated.[7] As we know, the oxyphilic Ln cations are easily combined with the surfaces of lacunary POM units, usually leading to precipitation rather than crystallization,[4b,15] while the reactions between POAs and TM ions are less active. As a result, when Ln and TM ions simultaneously react with POAs, the reaction competition will unavoidably exist among the strongly oxyphilic Ln cations and relatively less active TM ions in the reaction system.[8] However, we find that it is more difficult to control the syntheses of 3d-4f heterometallic POMs with mixed organic ligands than those with only one type of ligands in our exploration, which is mainly due to the fact that different organic ligands have different solubilities as well as different binding capabilities. Hence, we choose the hydrothermal method to exploit this system because it has been proved to be an effective method in making organic−inorganic hybrid POMs.[16] On one hand, because solubilities of materials increase under hydrothermal conditions, different organic ligands can be introduced. On the other hand, the reduced viscosity of water under hydrothermal conditions enhances the diffusion processes so that solvent extraction of solids and crystal growth from solution are favored; thus, the formation of good quality crystals is possible.[16a−d] Moreover, hydrothermal conditions are able to make the reaction shift from the thermodynamic to the kinetic so that the equilibrium phases are replaced by structurally more complicated metastable phases; that is, the metastable phases or intermediate phases can easily be captured under hydrothermal conditions.[16e−g] By a hydrothermal method, 3d-4f-heterometal cations and mixed organic ligands (en and 2,2′-bipy) were successfully introduced to our system. Six novel 3d-4f heterometallic phosphotungstates **1**−**6** with mixed organic ligands were successfully synthesized. To investigate the effect of different TM ions on structural diversity, when the Mn^{II}, Fe^{II}, Co^{II}, Ni^{II}, or Zn^{II} ions replaced the Cu^{II} ion under the same conditions, only some amorphous precipitates were obtained, which suggested that the TM ions played a key factor in the construction of products. In addition, experimental results showed that increasing or decreasing the amount of $LnCl_3$ was unfavorable to form the title compounds, suggesting that the amount of $LnCl_3$ played a key role in making the products. Notably, although $[\alpha\text{-}PW_9O_{34}]^{9-}$ as a precursor was introduced to the reactions, the products contain only $[\alpha\text{-}PW_{11}O_{39}]^{7-}$. When only $[\alpha\text{-}PW_{11}O_{39}]^{7-}$ was used as a precursor under the same conditions, to our regret, only some amorphous powders were obtained. On the contrary, only $[\alpha\text{-}PW_9O_{34}]^{9-}$ was used, the 3d-4f heterometallic phosphotungstates with en ligands were isolated, which are similar to the reported structures.[17] Therefore, $[\alpha\text{-}PW_9O_{34}]^{9-}$ and $[\alpha\text{-}PW_{11}O_{39}]^{7-}$ may play a synergistic role in the title compounds. Considering **6** is the only compound possessing the 3-D structure, in the paralleling experiments, **6** was taken as an example to investigate the influence of the ratio of PW_{11}/PW_9 and pH on the products. When the ratio of PW_{11}/PW_9 varied from 0.1 to 10 under the same conditions, however, only some amorphous powers were obtained, except that when the ratio was 10 and 5, two new 3d-4f substituted POMs were synthesized.[18a,b] In the meantime, the pH effect on the reaction system was also investigated. When the pH was adjusted to 4.0, 4.9, and 5.9 by en, respectively, three other new compounds were isolated.[18c−e] Therefore, the ratio of PW_{11}/PW_9 and the pH played an important role in the formation and crystallization of the products. As a result, the systematic exploration on 3d-4f substituted POMs still remains a great challenge to us. In the following time, we will continuously exploit the formation mechanism and the pertinent synthetic chemistry by means of some organic polycarboxylic ligands or different POMs.

Structural Descriptions. The experimental XRPD patterns for **1**−**6** are in good agreement with the simulated XRPD patterns from the single-crystal X-ray diffraction, demonstrating

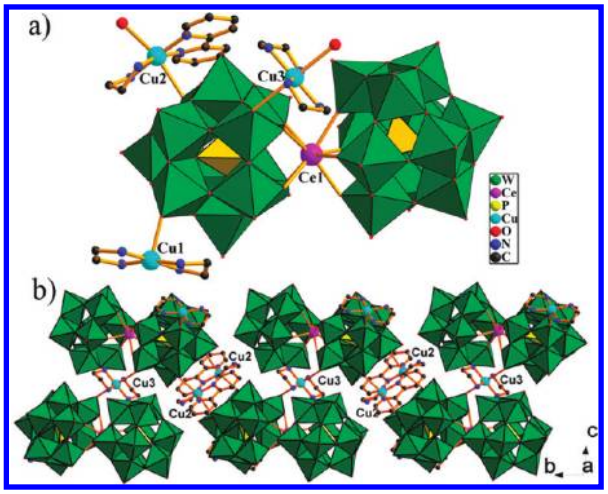

Figure 1. (a) Polyhedral/ball-and-stick representation of the structural unit of **1**. (b) 1-D chain built by alternate $[Ce(\alpha\text{-}PW_{11}O_{39})_2]^{11-}$ units, $[Cu3(en)_2]^{2+}$ and $[Cu2(en)(2,2'\text{-bipy})]^{2+}$ bridges. H atoms, lattice water molecules, and isolated $[enH_2]^{2+}$ and $[Cu4(en)_2]^{2+}$ are omitted for clarity.

the good phase purity for **1**−**6** (Figure S1 in the Supporting Information). The differences in intensity between the experimental and simulated XRPD patterns might be due to the variation in preferred orientation of the powder sample during collection of the experimental XRPD. Otherwise, the bond-valence calculations[19] indicate that all W atoms are in the +6 oxidation state, all Cu atoms are in the +2 oxidation state, and the Ln atoms are in the +3 oxidation state in **1**−**6**. Considering the charge balance of **1**−**6**, some protons need to be added. To locate the positions of these protons, the bond valence sum calculations of all the oxygen atoms on POM fragments are carried out (Figures S2−S7 and Tables S1−S6 in the Supporting Information). The Ln−O bond lengths (Table S7 in the Supporting Information) decrease with the early lanthanide series as the ionic radius of the Ln^{III} cations decreases, which is in accordance with the effect of the lanthanide contraction.[7,17b,20]

1 and **2** are isomorphous and crystallize in the triclinic space group $P\bar{1}$. Both consist of a 1-D chain constructed from sandwich-type bis(undecatungstophosphate)lanthanates $[Ln(\alpha\text{-}PW_{11}O_{39})_2]^{11-}$ (Ln = Ce^{III} for **1** and Pr^{III} for **2**) and $[Cu(en)_2]^{2+}$ and $[Cu(en)(2,2'\text{-bipy})]^{2+}$ units. Thus, only the structure of $(enH_2)_2[Cu(en)_2]\{[Cu(en)_2]_{1.5}[Cu(en)(2,2'\text{-bipy})]Ce[(\alpha\text{-}PW_{11}O_{39})_2]\}\cdot 2H_2O$ (**1**) is described here. The structural unit of **1** is composed of a sandwich-type $[Ce(\alpha\text{-}PW_{11}O_{39})_2]^{11-}$ POA, one and a half $[Cu(en)_2]^{2+}$, one $[Cu(en)(2,2'\text{-bipy})]^{2+}$, two protoned $[enH_2]^{2+}$ units, and two lattice water molecules (Figure 1a). Four independent copper ions (Cu1, Cu2, Cu3, and Cu4) exhibit three types of coordination geometries (Figure S8 in the Supporting Information). The $[Cu1(en)_2]^{2+}$ ion exhibits the square pyramid geometry with four nitrogen atoms from en ligands with Cu−N bond lengths ranging from 1.944(10) to 2.077(11) Å and one terminal oxygen atom from the $[Ce(\alpha\text{-}PW_{11}O_{39})_2]^{11-}$ POA with the Cu−O bond length 2.241(8) Å. The bridging $[Cu2(en)(2,2'\text{-bipy})]^{2+}$ ion locates in the octahedral geometry, which is coordinated by two nitrogen atoms from one en ligand with Cu−N distances 1.943(10)−2.105(10) Å and two nitrogen atoms from one 2,2′-bipy ligand with Cu−N distances 2.003(11)−2.020(10) Å, two terminal oxygen atoms from adjacent two $[Ce(\alpha\text{-}PW_{11}O_{39})_2]^{11-}$ POAs with Cu−O distances 2.467(8)−2.496(7) Å. The $[Cu3(en)_2]^{2+}$ ion forms an octahedral geometry defined by four nitrogen atoms from the chelating en ligands with Cu−N distances 1.988(13)−2.038(12) Å, two terminal oxygen atoms from adjacent two $[Ce(\alpha\text{-}PW_{11}O_{39})_2]^{11-}$ POAs with the Cu−O distances of 2.708(8) Å. The free $[Cu4(en)_2]^{2+}$ ion adopts the square geometry with four nitrogen atoms from two en ligands with Cu−N bond lengths ranging from 1.889(10) to 2.006(20) Å. The $[Ce(\alpha\text{-}PW_{11}O_{39})_2]^{11-}$ moiety is constructed from an eight-coordinate Ce^{III} cation sandwiched by two monovacant $[\alpha\text{-}PW_{11}O_{39}]^{7-}$ units, resulting in a well-known sandwich-type bis(undecatungstophospate) lanthanate structure, which was first discovered by Peacock and Weakley in 1971,[6] and this 1:2 structural series made up of one Ln cations and two monovacant Keggin-type POM units have been widely investigated.[3b,c,e,11b,11c,21] In the $[Ce(\alpha\text{-}PW_{11}O_{39})_2]^{11-}$ POA, the Ce^{III} cation incorporated to the monovacant site of the $[\alpha\text{-}PW_{11}O_{39}]^{7-}$ subunit in the "cap" region, adopting a distorted square antiprismatic coordination geometry (Figure S9a in the Supporting Information), bonding to eight oxygen atoms (O12, O15, O19, O28, O52, O65, O68, O72) from the monovacant sites of two adjacent $[\alpha\text{-}PW_{11}O_{39}]^{7-}$ units with Ce−O distances of 2.442(8)−2.562(8) Å, and the average of 2.486 Å. In the coordination polyhedron around the Ce^{III} cation, O12, O15, O19, O28 group and O52, O65, O68, O72 group constitute two bottom planes of the square antiprism and their standard deviations from their least-squares are 0.028 and 0.027 Å, respectively. The dihedral angle for the two bottom surfaces is 1.5°. The distances of the Ce^{III} cation and the two bottom surfaces are 1.319 and 1.344 Å, respectively. The above-mentioned data indicate that the square antiprism is somewhat distorted. In the $[Ce(\alpha\text{-}PW_{11}O_{39})_2]^{11-}$ POA, the P atoms reside in the center of PO_4 tetrahedra, which have been somewhat distorted, resulting from the removal of one $[W{=}O_t]^{4+}$ unit and the incorporation of the Ce^{III} cation into the monovacant POM subunit as compared to the saturated Keggin-type structures. The P−O bond lengths vary from 1.495(8) to 1.574(8) Å, and the O−P−O bond angles are in the range 107.6(4)−112.5(4)°. Similarly, all the WO_6 octahedra are distorted to some degree.

It is more interesting that adjacent $[Ce(\alpha\text{-}PW_{11}O_{39})_2]^{11-}$ POAs are connected by $[Cu(en)_2]^{2+}$ and $[Cu(en)(2,2'\text{-bipy})]^{2+}$ units, leading to a novel 1-D zigzag chain structure (Figure 1b). In addition, these 1-D chains along the *a*-axis are connected with each other through the strong hydrogen-bonding interactions ($d_{(N\cdots O)}$ = 2.730− 3.427 Å), generating the 2-D sheet structure (Figure S10 in the Supporting Information). To our knowledge, similar 1-D structures built by mono-Ln sandwiched POM groups and TM complex are very rare.[7,17] In comparison with $[\{Ln(PW_{11}O_{39})_2\}\{Cu_2(bpy)_2(\mu\text{-ox})\}]^{9-}$ reported by Liu et al.,[7] some obvious distinctions are observed in **1**: (1) **1** was prepared under hydrothermal conditions other than the conventional aqueous solution; (2) Adjacent $[Ce(\alpha\text{-}PW_{11}O_{39})_2]^{11-}$ POAs are linked by alternate $[Cu(en)_2]^{2+}$ and $[Cu(en)(2,2'\text{-bipy})]^{2+}$ units in **1**; in contrast, adjacent $[Ln(\alpha\text{-}PW_{11}O_{39})_2]^{11-}$ POAs in $[\{Ln(PW_{11}O_{39})_2\}\{Cu_2(bpy)_2(\mu\text{-ox})\}]^{9-}$ (ref 7) are interconnected by $[Cu_2(bpy)_2(\mu\text{-ox})]^{2+}$ bridges. (3) Most important of all, **1** was synthesized by reaction of $Na_9[\alpha\text{-}PW_9O_{34}]\cdot 16H_2O$ and $Na_7[\alpha\text{-}PW_{11}O_{39}]\cdot nH_2O$ with 3d-4f heterometals, en, and 2,2′-bipy while $[\{Ln(PW_{11}O_{39})_2\}\{Cu_2(bpy)_2(\mu\text{-ox})\}]^{9-}$ (ref 7) was obtained by reaction of $[Ln(\alpha\text{-}PW_{11}O_{39})_2]^{11-}$ with $[Cu_2(bpy)_2(\mu\text{-ox})]^{2+}$.

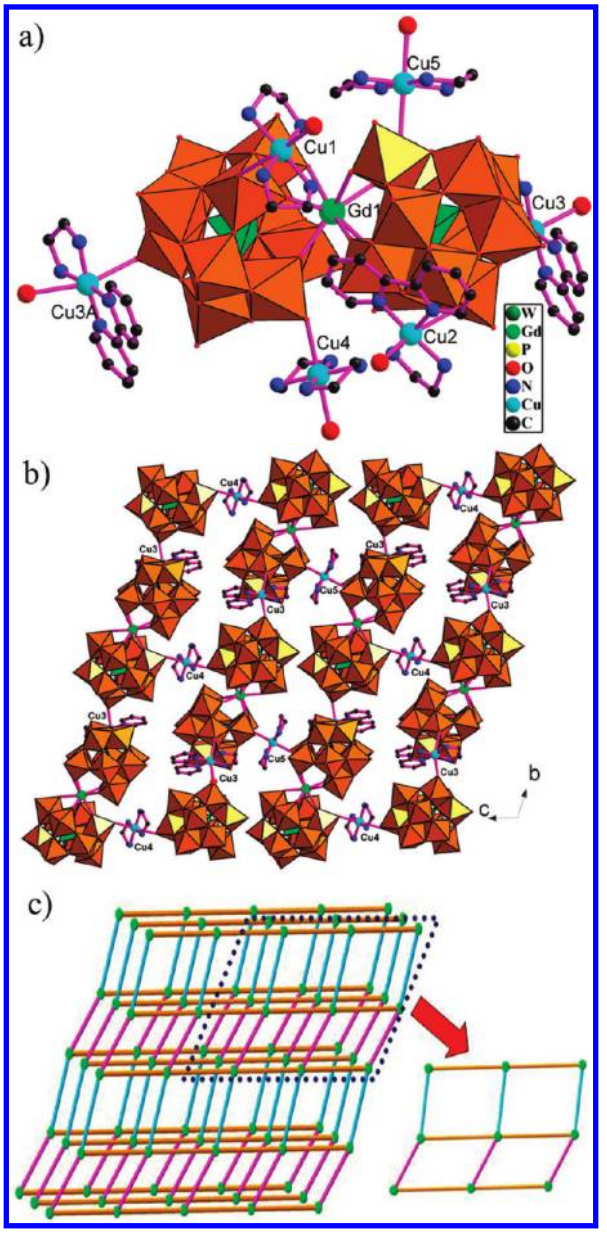

Figure 2. (a) Polyhedral/ball-and-stick representation of the structural unit of **3**. (b) 2-D network of **3**. (c) (4,4)-network showing the −AAA− mode. Color codes: $[Cu3(en)(2,2'\text{-bipy})]^{2+}$ bridge, light orange; $[Cu4(en)_2]^{2+}$ bridge, sky blue; $[Cu5(en)_2]^{2+}$ bridge, pink. H atoms, lattice water molecules and isolated $[Cu6(en)_2(H_2O)_2]^{2+}$ are omitted for clarity. The atom with the suffix A is generated by the symmetry operation: $-1 + x, -1 + y, z$.

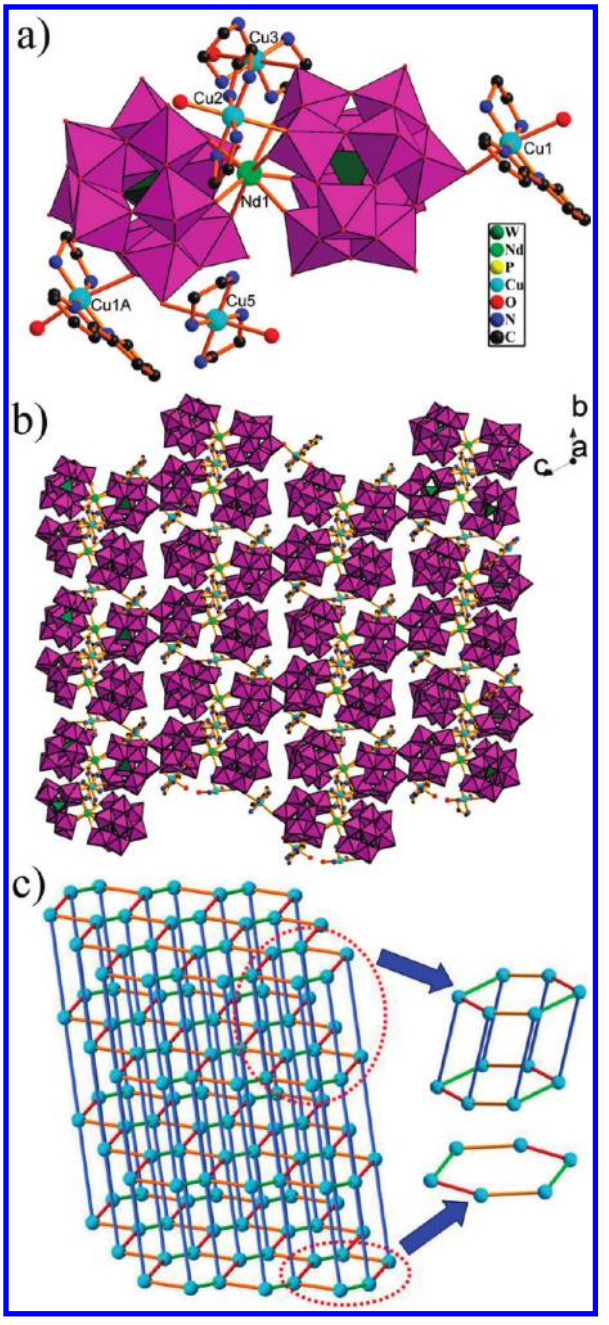

Figure 3. (a) Polyhedral/ball-and-stick representation of the molecular structural unit of **6**. (b) 3-D framework structure showing the −ABAB− mode. (c) $(4^6\cdot6^4)$ topology framework of **6**. Color codes: $[Cu1(en)(2,2'\text{-bipy})]^{2+}$ bridge, light blue; $[Cu2(en)_2]^{2+}$ bridge, bright green; $[Cu3(en)_2]^{2+}$ bridge, red; $[Cu5(en)_2]^{2+}$ bridge, light orange. H atoms, lattice water molecules and isolated $[Cu4(en)_2]^{2+}$ are omitted for clarity. The atom with the suffix A is generated by the symmetry operation: $x, -1 + y, -1 + z$.

3−**5** are isomorphous and crystallize in the triclinic $P\bar{1}$ space group; therefore, only $[Cu(en)_2(H_2O)_2][Cu(en)(2,2'\text{-bipy})(H_2O)]\{[Cu(en)_2]_2(H_2O)[Cu(en)(2,2'\text{-bipy})]Gd[(\alpha\text{-}HPW_{11}O_{39})_2]\}\cdot6H_2O$ (**3**) is discussed in detail. The structural unit of **3** consists of a sandwich-type $[Gd(\alpha\text{-}PW_{11}O_{39})_2]^{11-}$ POA, one $[Cu(en)(2,2'\text{-bipy})]^{2+}$, one $[Cu(en)_2]^{2+}$, one $[Cu(en)_2(H_2O)]^{2+}$, one isolated $[Cu(en)(2,2'\text{-bipy})(H_2O)]^{2+}$ and $[Cu(en)_2(H_2O)_2]^{2+}$, one proton, and six lattice water molecules (Figure 2a). Six crystallographic unique copper ions (Cu1, Cu2, Cu3, Cu4, Cu5, and Cu6) all exhibit the octahedral geometries (Figure S11 in the Supporting Information).The Gd^{III} cation in the $[Gd(\alpha\text{-}PW_{11}O_{39})_2]^{11-}$ unit exhibits a distorted square antiprismatic geometry (Figure S9b in the Supporting Information). Adjacent $[Gd(\alpha\text{-}PW_{11}O_{39})_2]^{11-}$ POAs are connected by $[Cu4(en)_2]^{2+}$ and $[Cu5(en)_2]^{2+}$ ions, giving rise to the 1-D infinite chain structure along the *b*-axis (Figure S12 in the Supporting Information). More interestingly, adjacent 1-D chains are linked together by $[Cu3(en)(2,2'\text{-bipy})]^{2+}$ and $[Cu3A(en)(2,2'\text{-bipy})]^{2+}$, leading to a 2-D layer structure (Figure 2b). As far as we know, the 2-D 3d-4f heterometallic POMs

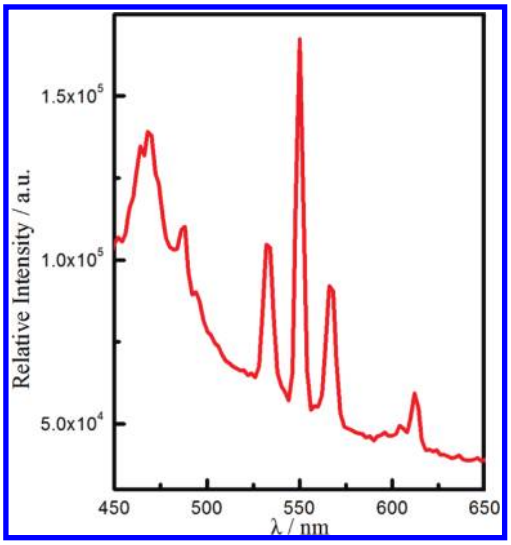

Figure 4. Photoluminescence spectrum of **4** at room temperature.

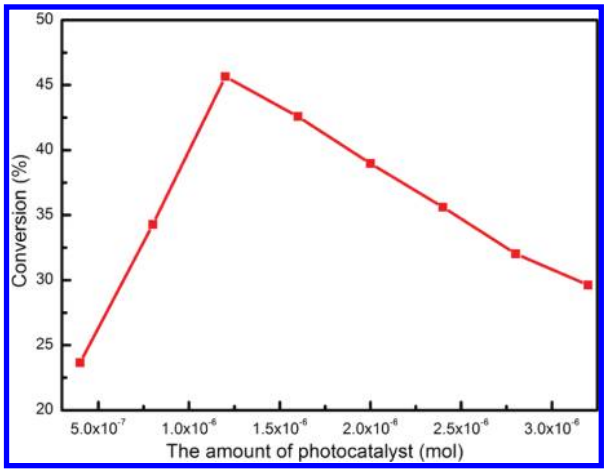

Figure 5. Conversion of RhB with different amounts of **5** as the photocatalyst upon 500 W Hg lamp irradiation for 3.5 h recorded in 25 mL of 2×10^{-5} mol·L^{-1} RhB solution.

containing mixed ligands have never been reported up to now. Topologically, each $\{[Cu(en)_2]_2(H_2O)[Cu(en)(2,2'\text{-bipy})]Gd[(\alpha\text{-}PW_{11}O_{39})_2]\}^{5-}$ unit is considered as a 4-connected node, with $[Cu3(en)(2,2'\text{-bipy})]^{2+}$, $[Cu4(en)_2]^{2+}$, and $[Cu5(en)_2]^{2+}$ as the bridges. The structure of **3** exhibits a (4,4)-topological network with the Schläfli symbol of $(4^4 \cdot 6^2)$ (Figure 2c).

6 belongs to the triclinic space group $P\bar{1}$. The structural unit of $Na_2[Cu(en)_2]_{0.5}\{[Cu(en)_2]_{1.5}[Cu(en)(2,2'\text{-bipy})]Nd[(\alpha\text{-}H_5PW_{11}O_{39})_2]\}\cdot 3H_2O$ (**6**) consists of one $\{[Cu(en)_2]_{1.5}[Cu(en)(2,2'\text{-bipy})]Nd[(\alpha\text{-}H_5PW_{11}O_{39})_2]\}^{3-}$ POA (Figure 3a), a half $[Cu(en)_2]^{2+}$, two sodium ions, five protons, and three lattice water molecules. The $[Cu1(en)(2,2'\text{-bipy})]^{2+}$, $[Cu2(en)_2]^{2+}$, $[Cu3(en)_2]^{2+}$, and $[Cu5(en)_2]^{2+}$ ions display the octahedral geometries whereas the free $[Cu4(en)_2]^{2+}$ ion exhibits a square geometry (Figure S13 in the Supporting Information).

The Nd^{III} cation in the $[Nd(\alpha\text{-}PW_{11}O_{39})_2]^{11-}$ unit displays the distorted square antiprismatic geometry (Figure S9c in the Supporting Information). The intriguing feature of **6** is that each $[Nd(\alpha\text{-}PW_{11}O_{39})_2]^{11-}$ subunit acts as a pentadentate ligand to link one $[Cu1(en)(2,2'\text{-bipy})]^{2+}$ ion, one $[Cu1A(en)(2,2'\text{-bipy})]^{2+}$ ion, one $[Cu2(en)_2]^{2+}$ ion, one $[Cu3(en)_2]^{2+}$ ion, and one $[Cu5(en)_2]^{2+}$ ion via five terminal oxygen atoms (O2, O40, O7, O8, and O47, respectively), forming the 2-D network structure (Figure S14 in the Supporting Information). Most interestingly, adjacent layers are interconnected by bridging O7−Cu2−O7 connectors, leading to a fascinating 3-D framework (Figure 3b). Topologically, if each $\{[(\alpha\text{-}PW_{11}O_{39})_2]Nd[Cu(en)_2]_{1.5}[Cu(en)(2,2'\text{-bipy})]\}^{8-}$ unit is viewed as a 5-connected node, and $[Cu1(en)(2,2'\text{-bipy})]^{2+}$, $[Cu2(en)_2]^{2+}$, $[Cu3(en)_2]^{2+}$, and $[Cu5(en)_2]^{2+}$ act as the bridges, the structure of **6** can be described as a 5-connected framework with the Schläfli symbol $(4^6 \cdot 6^4)$ (Figure 3c).

Photoluminescence Property. Generally, Ln cations have low molar absorptivity, which results in weak emission when directly excited.[22a] They can exhibit extremely sharp emission bands attributed to their 4f electrons, which are responsible for their properties.[22b] However, effective characteristic emission of Ln cations can be observed by employing appropriate ligands that can absorb and transfer the energy to Ln cations.[22c,d] Ln cations can emit a photon or relax via a series of nonradiative processes, which is known as the "antenna effect".[23] The solid-state photoluminescence spectrum of **4** was investigated at room temperature upon photoexcitation (Figure 4), as all the transitions to the ground-state ^7F_J (J = 6, 5, 4, 3) manifold from the $^5D_4$ excited state of the Tb^{III} ion are usually evident when excited at 366 nm. However, some obvious distinctions are found in **4** compared with the previous results of Tb^{III} ions.[24] Several emission bands at approximately 464, 468, and 532 nm have been observed in **4**, except that the characteristic emission bands of the Tb^{III} ion are in the visible region at 487 nm ($^5D_4 \rightarrow {}^7F_6$), 550 nm ($^5D_4 \rightarrow {}^7F_5$), 567 nm ($^5D_4 \rightarrow {}^7F_4$), and 611 nm ($^5D_4 \rightarrow {}^7F_3$), respectively. The emission wavelength at 550 nm is the most intense, which is comparable with the previous results of Tb^{III} ions.[24] In order to further investigate the reason, we measured the solid-state photoluminescence spectra of the free 2,2′-bipy and the precursor $Na_7[\alpha\text{-}PW_{11}O_{39}]\cdot nH_2O$ at the same conditions (Figure S15 in the Supporting Information). In comparison with the case of 2,2′-bipy, the emission bands at 464 and 468 nm are assigned to the intraligand $\pi-\pi^*$ transitions of 2,2′-bipy ligands and the ligand-to-metal-charge-transfer transitions.[25] Compared to the case of the precursor $Na_7[\alpha\text{-}PW_{11}O_{39}]\cdot nH_2O$, the emission bands at 532 nm may be attributed to the O → W transition and/or the split of the $^5D_4 \rightarrow {}^7F_J$.[26] In fact, the intramolecular energy transfer of the O → W transitions in POMs has been investigated by Yamase et al.;[27] this charge-transfer band plays an important role in the luminescence of **4**, which is consistent with the previous report for a SbW_6/DODA LB film and a $K\cdot SbW_6$ solid.[28]

Photocatalysis. Photodegradation reactions of RhB upon 500 W Hg lamp irradiation in the presence of **1**, **2**, **3**, **4**, **5**, or **6** as the photocatalyst have been examined by UV−visible spectroscopy. The target substrate RhB contains four *N*-ethyl groups at either side of the xanthene ring, which is stable in aqueous solutions upon visible-light irradiation.[29] When RhB substrates were kept in darkness either in the presence of or in the absence of **1**, **2**, **3**, **4**, **5**, or **6**, the degradation reactions of RhB hardly happened (Figure S16 in the Supporting Information). When RhB substrates were kept upon 500 W Hg lamp irradiation in the presence of **1**, **2**, **3**, **4**, **5**, or **6**, the photodegradation reactions of RhB happened. In order to select the optimum usage amount of the photocatalyst, **5** was taken as an example to study by adding 4×10^{-7}, 8×10^{-7}, 1.2×10^{-6}, 1.6×10^{-6}, 2.0×10^{-6}, $2.4 \times$

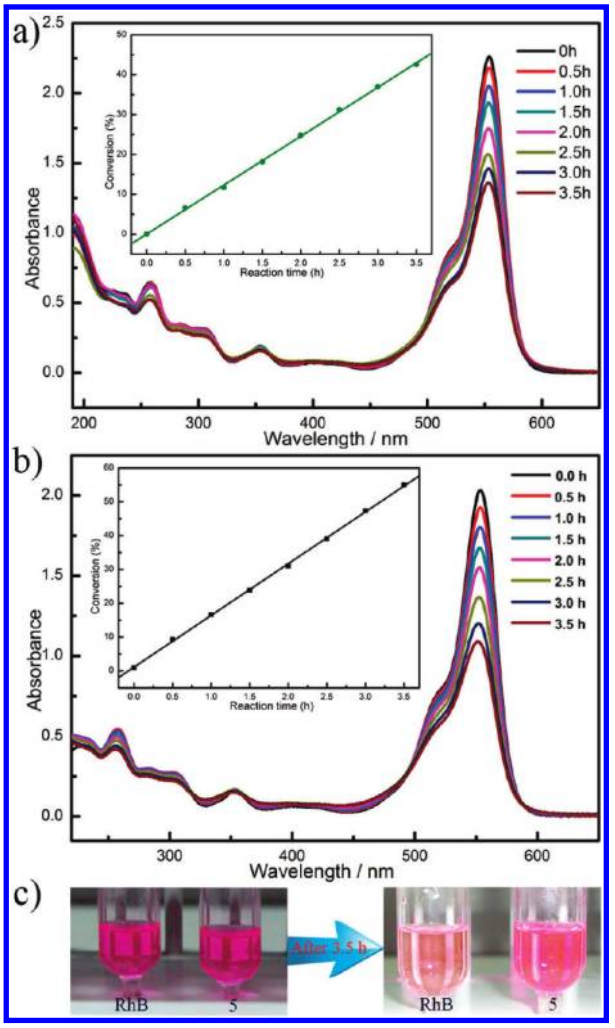

Figure 6. (a) UV−vis absorption spectra vary with **5** recorded in the solution including 2×10^{-5} mol·L^{-1} RhB and 1.2×10^{-6} mol sample **5**. (b) Photodegradation reaction of RhB in the absence of **5** upon 500 W Hg lamp irradiation. Inset: conversion of RhB (K) with the reaction time (t) of **5**. The conversion of RhB (K) can be expressed as $K = (I_0 - I_t)/I_0$, where I_0 represents the UV−vis intensity of RhB at the initial time ($t = 0$) and I_t is the UV−vis absorption intensity at a given time (t). (c) The color of the solution of RhB and in the presence of **5** changes as the irradiation time increases.

10^{-6}, 2.8×10^{-6}, or 3.2×10^{-6} mol to a 25 mL solution of RhB (2×10^{-5} mol·L^{-1}) upon 500 W Hg lamp irradiation for 3.5 h, respectively. The results show that the optimum usage amount of **5** is 1.2×10^{-6} mol (Figure 5). Under this condition, the influence of the irradiation time on the photodegradation reaction of RhB has also been investigated by UV−visible spectra (Figure 6a). The results show that the absorbance of UV−visible spectra decreases as the irradiation time increases, which explains that RhB gradually photodegrades and the amount of RhB in solution is less and less. In comparison with the photodegradation reaction of RhB in the absence of **5** upon 500 W Hg lamp irradiation (Figure 6b), the decline of the absorbance of UV−visible spectra in the presence of **5** is slower than that in the absence of **5**, suggesting that the photocatalyst **5** can prohibit the photodegradation of RhB. Moreover, the comparison of the color change of the solution in the presence of **5** or in the absence of **5** before and after the reactions can also support this conclusion (Figure 6c). In addition, we choose the characteristic absorption band of RhB (around 554 nm), and the fact that the plot of the conversion of RhB (K) varies with reaction time (t) can also consolidate this point (inset of Figure 6a). The conversion of RhB (K) can be expressed as $K = (I_0 - I_t)/I_0$, where I_0 represents the UV−vis intensity of RhB at the initial time ($t = 0$) and I_t is the UV−vis absorption intensity at a given time (t). The conversion of RhB in the absence of **5** upon irradiation for 3.5 h is 51% while the conversion of RhB in the presence of **5** is 46%, which also indicates that **5** can prohibit the photodegradation of RhB. (Similar results for **1**−**4** and **6** are included in Figure S17 in the Supporting Information.) In addition, because **3**, **4**, and **5** are isostructural, their photodegradation effects on RhB are compared. Under the same conditions as those for **5**, the conversions of **3**, **4**, and **5** are 29%, 35%, and 46%, which suggest that the photodegradation of RhB increases as the ionic radius of Ln^{III} cations increases. A similar result also can be observed for **1** (26%) and **2** (34%) (Figure S17 in the Supporting Information). Since **1**−**6** have different structural types, we cannot observe the general law. However, each structural type shows the law that the photodegradation of RhB increases as the ionic radius of Ln^{III} cations increases, which suggests that Ln^{III} cations may play an important role in inhibiting the photodegradation of RhB. In a word, the main reasons why **1**−**6** can inhibit the photodegradation of RhB may be as follows: (i) one of the possible reasons for the inhibition effect of the photodegradation of RhB is that compounds **1**−**6** can work as absorbers of the Hg lamp irradiation. (ii) the hydrogen-bonding interactions between donors and acceptors in RhB substrates ($N(C_2H_5)_2$, COOH) and **1**−**6** (en, surface oxygen atoms of POMs) and the weak $\pi-\pi$ stacking interactions between phenyl cycles on RhB substrates and pyridine cycles on 2,2′-bipy ligands in **1**−**6** enhance the chemical stability of RhB substrates in the solutions, which leads to the slow photodegradation of RhB substrates. Currently, detailed study on the mechanism of photocatalysis of RhB in the presence of **1**−**6** as the photocatalyst is in progress.

CONCLUSIONS

In conclusion, six novel organic−inorganic hybrid derivatives **1**−**6** with two types of organic ligands have been hydrothermally synthesized and structurally characterized by elemental analyses, ICP, XRPD, IR spectra, UV−vis spectra, EPR spectra, TG analyses, and single-crystal X-ray diffraction. The common features of **1**−**6** are that they all consist of sandwich-type $[Ln(\alpha\text{-}PW_{11}O_{39})_2]^{11-}$ POAs and copper coordination cations. **1** and **2** show 1-D zigzag chains and **3**−**5** exhibit unprecedented 2-D structures built by $[Ln(\alpha\text{-}PW_{11}O_{39})_2]^{11-}$ POAs, $[Cu(en)_2]^{2+}$, and $[Cu(en)(2,2'\text{-bipy})]^{2+}$ cations, whereas **6** displays the rare 3-D framework with a $(4^6 \cdot 6^4)$ topology. The photoluminescence of **4** is assigned to the combination effect of the Tb^{III} ion, 2,2′-bipy ligands, and the oxygen-to-metal charge transfer. The photocatalytic properties of **1**−**6** have been examined. The following work will focus on synthesizing more multidimensional organic−inorganic hybrids consisting of 3d-4f heterometals and POM units by means of introducing other organic polycarboxylic ligands or different POMs.

ASSOCIATED CONTENT

Supporting Information. Representations of XPRD patterns, IR spectra, UV spectra, The solid-state emission spectra of

dx.doi.org/10.1021/cg2001249 |*Cryst. Growth Des.* 2011, 11, 3769–3777

$Na_7[\alpha\text{-}PW_{11}O_{39}]\cdot nH_2O$ and 2,2′-bipy, EPR spectra for **2**, **4**, and **5**, the UV−visible spectra of RhB photodegradation upon the 500 W Hg lamp irradiation in the presence of **1**, **2**, **3**, **4**, **5**, or **6**, TGA curve and X-ray crystallographic data of **1**−**6** in CIF format. This material is available free of charge via the Internet at http://pubs.acs.org.

AUTHOR INFORMATION

Corresponding Author

*Fax: (+86) 378 3886876. E-mail: jpwang@henu.edu.cn.

ACKNOWLEDGMENT

This work was supported by the Natural Science Foundation of China, Special Research Fund for the Doctoral Program of Higher Education, Innovation Scientists and Technicians Troop Construction Projects of Henan Province, and the Natural Science Foundation of Henan Province.

REFERENCES

(1) (a) Müller, A.; Serain, C. *Acc. Chem. Res.* **2000**, *33*, 2–10. (b) Rhule, J. T.; Neiwert, W. A.; Hardcastle, K. I.; Do, B. T.; Hill, C. L. *J. Am. Chem. Soc.* **2001**, *123*, 12101–12102. (c) Ruether, T.; Hultgren, V. M.; Timko, B. P.; Bond, A. M.; Jackson, W. R.; Wedd, A. G. *J. Am. Chem. Soc.* **2003**, *125*, 10133–10143. (d) Bareyt, S.; Piligkos, S.; Hasenknopf, B.; Gouzerh, P.; Lacote, E.; Thorimbert, S.; Malacria, M. *J. Am. Chem. Soc.* **2005**, *127*, 6788–6794. (e) Mialane, P.; Duboc, C.; Marrot, J.; Rivière, E.; Dolbecq, A.; Sécheresse, F. *Chem.—Eur. J.* **2006**, *12*, 1950–1959. (f) An, H. Y.; Wang, E. B.; Xiao, D. R.; Li, Y. G.; Su, Z. M.; Xu, L. *Angew. Chem., Int. Ed.* **2006**, *45*, 904–908. (g) Bassil, B. S.; Dickman, M. H.; Römer, I.; Kammer, B. v. d.; Kortz, U. *Angew. Chem., Int. Ed.* **2007**, *46*, 6192–6195. (h) Long, D. L.; Tsunashima, R.; Cronin, L. *Angew. Chem., Int. Ed.* **2010**, *49*, 1736–1758.

(2) (a) Kato, C. N.; Shinohara, A.; Hayashi, K.; Nomiya, K. *Inorg. Chem.* **2006**, *45*, 8108–8119. (b) Hou, Y.; Fang, X. K.; Hill, C. L. *Chem.—Eur. J.* **2007**, *13*, 9442–9447. (c) Lahootun, V.; Besson, C.; Villanneau, R.; Villain, F.; Chamoreau, L. M.; Boubekeur, K.; Blanchard, S.; Thouvenot, R.; Proust, A. *J. Am. Chem. Soc.* **2007**, *129*, 7127–7135. (d) Nogueira, H. I. S.; Almeida Paz, F. A.; Teixeira, P. A. F.; Klinowski, J. *Chem. Commun.* **2006**, 2953–2955. (e) Mialane, P.; Dolbecq, A.; Rivière, E.; Marrot, J.; Sécheresse, F. *Angew. Chem., Int. Ed.* **2004**, *43*, 2274–2277. (f) Kortz, U.; Hussain, F.; Reicke, M. *Angew. Chem., Int. Ed.* **2005**, *44*, 3773–3777. (g) Zhang, Z. M.; Qi, Y. F.; Qin, C.; Li, Y. G.; Wang, E. B.; Wang, X. L.; Su, Z. M.; Xu, L. *Inorg. Chem.* **2007**, *46*, 8162–8169.

(3) (a) Peacock, R. D.; Weakley, T. J. R. *J. Chem. Soc. A* **1971**, 1836–1839. (b) Sadakane, M.; Dickman, M. H.; Pope, M. T. *Angew. Chem., Int. Ed. Engl.* **2000**, *39*, 2914–2916. (c) Mialane, P.; Dolbecq, A.; Rivière, E.; Marrot, J.; Sècheresse, F. *Eur. J. Inorg. Chem.* **2004**, 33–36. (d) Sousa, F. L.; Paz, F. A. A.; Cavaleiro, A. M. V.; Klinowski, J.; Nogueira, H. I. S. *Chem. Commun.* **2004**, 2656–2657. (e) Bassil, B. S.; Dickman, M. H.; von der Kammer, B.; Kortz, U. *Inorg. Chem.* **2007**, *46*, 2452–2458.

(4) (a) Li, Y. W.; Li, Y. G.; Wang, Y. H.; Feng, X. J.; Lu, Y.; Wang, E. B. *Inorg. Chem.* **2009**, *48*, 6452–6458. (b) Yao, S.; Zhang, Z. M.; Li, Y. G.; Lu, Y.; Wang, E. B.; Su, Z. M. *Cryst. Growth Des.* **2010**, *10*, 135–139. (c) Fang, X. K.; Kögerler, P. *Angew. Chem., Int. Ed.* **2008**, *47*, 8123–8126. (d) Fang, X. K.; Kögerler, P. *Chem. Commun.* **2008**, 3396–3398. (e) Pang, H. J.; Zhang, C. J.; Shi, D. M.; Chen, Y. G. *Cryst. Growth Des.* **2008**, *8*, 4476–4480.

(5) (a) Zhao, B.; Cheng, P.; Chen, X. Y.; Cheng, C.; Shi, W.; Liao, D. Z.; Yan, S. P.; Jiang, Z. H. *J. Am. Chem. Soc.* **2004**, *126*, 3012–3013. (b) Novitchi, G.; Wernsdorfer, W.; Chibotaru, L. F.; Costes, J. P.; Anson, C. E.; Powell, A. K. *Angew. Chem., Int. Ed.* **2009**, *48*, 1614–1619. (c) Huang, Y. G.; Jiang, F. L.; Hong, M. C. *Coord. Chem. Rev.* **2009**, *253*, 2814–2834. (d) Cai, Y. P.; Zhou, X. X.; Zhou, Z. Y.; Zhu, S. Z.; Thallapally, P. K.; Liu, J. *Inorg. Chem.* **2009**, *48*, 6341–6343. (e) Zhou, Y. F.; Hong, M. C.; Wu, X. T. *Chem. Commun.* **2006**, 135–143. (f) Hu, X.; Zeng, Y. F.; Chen, Z.; Sañudo, E. C.; Liu, F. C.; Ribas, J.; Bu, X. H. *Cryst. Growth Des.* **2009**, *9*, 421–426.

(6) Merca, A.; Müller, A.; Slageren, J. V.; Läge, M.; Krebs, B. *J. Cluster Sci.* **2007**, *18*, 711–719.

(7) Cao, J. F.; Liu, S. X.; Cao, R. G.; Xie, L. H.; Ren, Y. H.; Gao, C. Y.; Xu, L. *Dalton Trans.* **2008**, 115–120.

(8) (a) Chen, W. L.; Li, Y. G.; Wang, Y. H.; Wang, E. B.; Zhang, Z. M. *Dalton Trans.* **2008**, 865–867. (b) Chen, W. L.; Li, Y. G.; Wang, Y. H.; Wang, E. B. *Eur. J. Inorg. Chem.* **2007**, 2216–2220. (c) Zhang, Z. M.; Li, Y. G.; Chen, W. L.; Wang, E. B.; Wang, X. L. *Inorg. Chem. Commun.* **2008**, *11*, 879–882.

(9) (a) Nohra, B.; Mialane, P.; Dolbecq, A.; Rivière, E.; Marrot, J.; Sécheresse, F. *Chem. Commun.* **2009**, 2703–2705. (b) Compain, J. D.; Mialane, P.; Dolbecq, A.; Mbomekallé, I. M.; Marrot, J.; Sécheresse, F.; Duboc, C.; Rivière, E. *Inorg. Chem.* **2010**, *49*, 2851–2858.

(10) Reinoso, S.; Galán Mascarós, J. R. *Inorg. Chem.* **2010**, *49*, 377–379.

(11) (a) Niu, J. Y.; Zhao, J. W.; Wang, J. P. *Inorg. Chem. Commun.* **2004**, *7*, 876–879. (b) Wang, J. P.; Duan, X. Y.; Du, X. D.; Niu, J. Y. *Cryst. Growth Des.* **2006**, *6*, 2266–2270. (c) Wang, J. P.; Zhao, J. W.; Duan, X. Y.; Niu, J. Y. *Cryst. Growth Des.* **2006**, *6*, 507–513. (d) Niu, J. Y.; Wang, K. H.; Chen, H. N.; Zhao, J. W.; Ma, P. T.; Wang, J. P.; Li, M. X.; Bai, Y.; Dang, D. B. *Cryst. Growth Des.* **2009**, *9*, 4362–4372.

(12) Li, B.; Zhao, J. W.; Zheng, S. T.; Yang, G. Y. *Inorg. Chem.* **2009**, *48*, 8294–8303.

(13) (a) Brevard, C.; Schimpf, R.; Tourne, C. M. *J. Am. Chem. Soc.* **1983**, *105*, 7059–7063. (b) Domaille, P. J. *Inorg. Synth.* **1990**, *27*, 100–101.

(14) (a) Sheldrick, G. M. *SHELXS97, Program for Crystal Structure Solution*; University of Göttingen: Göttingen, Germany, 1997. (b) Sheldrick, G. M. *SHELXL97, Program for Crystal Structure Refinement*; University of Göttingen: Göttingen, Germany, 1997.

(15) (a) Howell, R. C.; Perez, F. G.; Jain, S.; Horrocks, W. D.; Rheingold, A. L.; Francesconi, L. C. *Angew. Chem., Int. Ed.* **2001**, *40*, 4031–4034. (b) Bassil, B. S.; Dickman, M. H.; Römer, I.; Kammer, B.; Kortz, U. *Angew. Chem., Int. Ed.* **2007**, *46*, 6192–6195. (c) Boglio, C.; Micoine, K.; Rémy, P.; Hasenknopf, B.; Thorimbert, S.; Lacôte, E.; Malacria, M.; Afonso, C.; Tabet, J. C. *Chem.—Eur. J.* **2007**, *13*, 5426–5432.

(16) (a) Laudise, R. A. *Prog. Inorg. Chem.* **1962**, *3*, 1–47. (b) Rabenau, A. *Angew. Chem., Int. Ed. Engl.* **1985**, *24*, 1026–1040. (c) Laudise, R. A. *Chem. Eng. News* **1987**, *65*, 30–43. (d) Hagrman, P. J.; Hagrman, D.; Zubietua, J. *Angew. Chem., Int. Ed.* **1999**, *38*, 2638–2684. (e) Gopalakrishnan, J. *Chem. Mater.* **1995**, *7*, 1265–1275. (f) Zhao, J. W.; Wang, C. M.; Zhang, J.; Zheng, S. T.; Yang, G. Y. *Chem.—Eur. J.* **2008**, *14*, 9223–9239. (g) Zhao, J. W.; Zhang, H. P.; Jia, J.; Zheng, S. T.; Yang, G. Y. *Chem.—Eur. J.* **2007**, *13*, 10030–10045.

(17) (a) Li, B.; Zhao, J. W.; Zheng, S. T.; Yang, G. Y. *J. Cluster Sci.* **2009**, *20*, 503–513. (b) Du, D. Y.; Qin, J. S.; Li, S. L.; Wang, X. L.; Yang, G. S.; Li, Y. G.; Shao, K. Z.; Su, Z. M. *Inorg. Chem. Acta* **2010**, *363*, 3823–3831.

(18) (a) Triclinic, space group $P\bar{1}$, a = 12.947(9) Å, b = 19.300(13) Å, c = 21.453(14) Å, α = 95.946(14)°, β = 95.196(14)°, γ = 95.798(15)°, V = 5277(6) Å^3. (b) Triclinic, space group $P\bar{1}$, a = 15.974(8) Å, b = 18.036(13) Å, c = 20.937(10) Å, α = 113.761(9)°, β = 90.915(9)°, γ = 94.552(9)°, V = 5496(5) Å^3. (c) Monolinic, space group $C2/c$, a = 21.751(2) Å, b = 27.263(3) Å, c = 21.987(3) Å, β = 114.982(2)°, V = 11818(2) Å^3. (d) Triclinic, space group $P\bar{1}$, a = 11.991(3) Å, b = 17.564(5) Å, c = 27.010(7) Å, α = 94.662(8)°, β = 98.084(5)°, γ = 103.359(8)°, V = 5441(2) Å^3. (e) Triclinic, space group $P\bar{1}$, a = 13.179(4) Å, b = 22.716(7) Å, c = 25.962(8) Å, α = 105.925(7)°, β = 101.375(7)°, γ = 94.586(7)°, V = 7253(4) Å^3.

(19) Brown, I. D.; Altermatt, D. *Acta Crystallogr.* **1985**, *B41*, 244–247.

(20) (a) Ozeki, T.; Yamase, T. *Acta Crystallogr., Sect. B* **1994**, *B50*, 128–134. (b) López, X.; Bo, C.; Poblet, J. M. *J. Am. Chem. Soc.*

2002, *124*, 12574–12582. (c) Gautier, R.; Andersen, O. H.; Gougeon, P.; Halet, J. F.; Canadell, E.; Martin, D. D. *Inorg. Chem.* **2002**, *41*, 4689–4699.

(21) Mialane, P.; Lisnard, L.; Mallard, A.; Marrot, J.; Antic Fidancev, E.; Aschehoug, P.; Vivien, D.; Sécheresse, F. *Inorg. Chem.* **2003**, *42*, 2102–2108.

(22) (a) Mahata, P.; Ramya., K. V.; Natarajan, S. *Chem.—Eur. J.* **2008**, *14*, 5839–5850. (b) Kido, J. J.; Okamoto, Y. S. *Chem. Rev.* **2002**, *102*, 2357–2368. (c) Chandler, B. D.; Yu, J. Q.; Cramb, D. T.; Shimizu, G. K. H. *Chem. Mater.* **2007**, *19*, 4467–4473. (d) de Lill, D. T.; de Bettencourt Dias, A.; Cahill, C. L. *Inorg. Chem.* **2007**, *46*, 3960–3965.

(23) (a) Blasse, G.; Grabmaier, B. C. *Luminescent Materials*; Springer: Berlin, 1994. (b) Chandler, B. D.; Cramb, D. T.; Shimizu, G. K. H. *J. Am. Chem. Soc.* **2006**, *128*, 10403–10412. (c) Selvin, P. R. *Nat. Struct. Biol.* **2000**, *7*, 730–734. (d) Whan, R. E.; Crosby, G. A. *J. Mol. Spectrosc.* **1962**, *8*, 315–327.

(24) (a) Ritchie, C.; Moore, E. G.; Speldrich, M.; Kögerler, P.; Boskovic, C. *Angew. Chem., Int. Ed.* **2010**, *49*, 7702–7705. (b) Mahata, P.; Ramya, K. V.; Natarajan, S. *Chem.—Eur. J.* **2008**, *14*, 5839–5850. (c) Tang, S. F.; Song, J. L.; Li, X. L.; Mao, J. G. *Cryst. Growth Des.* **2006**, *6*, 2322–2326.

(25) (a) Batey, H. D.; Whitwood, A. C.; Duhme Klair, A. K. *Inorg. Chem.* **2007**, *46*, 6516–6528. (b) Lan, Y. Q.; Li, S. L.; Wang, X. L.; Shao, K. Z.; Su, Z. M.; Wang, E. B. *Inorg. Chem.* **2008**, *47*, 529–534. (c) Sun, C. Y.; Li, Y. G.; Wang, E. B.; Xiao, D. R.; An, H. Y.; Xu, L. *Inorg. Chem.* **2007**, *46*, 1563–1574.

(26) (a) Filipescu, N.; Sager, W. F.; Serafin, F. A. *J. Phys. Chem.* **1964**, *68*, 3324–3346. (b) Wang, Y. H.; Wang, X. L.; Hu, C. W. *J. Colloid Interface Sci.* **2002**, *249*, 307–315.

(27) (a) Yamase, T. *Chem. Rev.* **1998**, *98*, 3–49. (b) Creaser, I.; Heckel, M. C.; Neitz, R. J.; Pope, M. T. *Inorg. Chem.* **1993**, *32*, 1573–1578. (c) Yamase, T.; Naruke, H. *J. Chem. Soc., Dalton Trans.* **1991**, 285–292. (d) Ballardini, R.; Chiorboli, E.; Balzani, V. *Inorg. Chim. Acta* **1984**, *95*, 323–327. (e) Wang, X. L.; Guo, Y. Q.; Li, Y. G.; Wang, E. B.; Hu, C. W.; Hu, N. H. *Inorg. Chem.* **2003**, *42*, 4135–4140.

(28) (a) Yamase, T.; Naruke, H.; Sasaki, Y. *J. Chem. Soc., Dalton Trans.* **1990**, 1687–1696. (b) Xu, L.; Zhang, H. Y.; Wang, E. B.; Kurth, D. G.; Li, Z. *J. Mater. Chem.* **2002**, *12*, 654–657. (c) Zhang, T. R.; Spitz, C.; Antonietti, M.; Faul, C. F. J. *Chem.—Eur. J.* **2005**, *11*, 1001–1009.

(29) (a) Tao, X.; Ma, W. H.; Zhang, T. Y.; Zhao, J. C. *Chem.—Eur. J.* **2002**, *8*, 1321–1326. (b) Chen, C. C.; Zhao, W.; Lei, P. X.; Zhao, J. C.; Serpone, N. *Chem.—Eur. J.* **2004**, *10*, 1956–1965. (c) Wu, Q.; Chen, W. L.; Liu, C.; Li, Y. G.; Lin, S. W.; Wang, E. B. *Dalton Trans.* **2011**, *40*, 56–61. (d) Wang, S. M.; Chen, W. L.; Wang, E. B.; Li, Y. G.; Feng, X. J.; Liu, L. *Inorg. Chem. Commun.* **2010**, *13*, 972–975. (e) Chen, W. L.; Chen, B. W.; Tan, H. Q.; Li, Y. G.; Wang, Y. H.; Wang, E. B. *J. Solid State Chem.* **2010**, *183*, 310–321.